MICROSTRUCTURE OF Cu2O DEFORMED SINGLE CRYSTALS

E. Fries, C. Marhic, T. Bretheau

MICROSTRUCTURE OF Cu_2O DEFORMED SINGLE CRYSTALS

E. FRIES, C. MARHIC, T. BRETHEAU

Laboratoire de Physique des Matériaux, C. N. R. S. Bellevue,
92190 Meudon, France

Résumé. — Des monocristaux d'oxyde de cuivre Cu_2O ont été déformés par compression à haute température ($T > 0{,}5\ T_f$) pour étudier la relation entre fluage et microstructure. La force a été appliquée parallèlement à [100], la déformation variant de 2 % à 30 %. Les rotations de réseau et la structure cellulaire ont été étudiées par topographie de rayons X Berg-Barrett et attaque chimique. L'étude du régime transitoire montre quatre plans de glissement $\{ 011 \} < 01\bar{1} >$ qui contribuent à la mise en place d'une sous-structure de fluage en régime stationnaire. La taille moyenne des cellules est de 50 μm pour une déformation de 30 %. La déformation se fait par glissement double.

Abstract. — Cuprous oxide crystals have been deformed in high temperature compression ($T > 0.5\ T_m$) in order to study the relation between creep and microstructure. The stress has been applied parallel to [100] with various strains from about 2 % to 30 %. Berg-Barrett X ray topography and chemical etching have been used to study lattice rotations and cell structure. In the transient state we have found four glide systems $\{ 011 \} < 01\bar{1} >$ giving rise to a characteristic creep microstructure in the steady state creep. The cell size is 40 μm after a 30 % strain. The deformation is associated with a double slip.

1. **Introduction.** — Cu_2O cuprite ceramic oxide has physical properties strongly bound to non-stoichiometry and a fairly low molten temperature (1 230 °C). We were interested in the microstructure of this oxide along with high temperature creep ($T > 0.5\ T_m$). The present study can be considered in a more general investigation of the mechanical behavior of cuprite single crystals : the slip systems along with Cu_2O plastic deformation at low temperature have been studied by Martinez-Clemente *et al.* [1]. The results of high temperature creep mechanical tests will be published by Bretheau *et al.* [2]. Here we have used the classical Berg-Barrett X ray topography [3, 4] to observe creep microstructure ; it allows scale sample observations (magnification 20 to 100). Indeed, the evolution of dislocation substructure and resultant lattice rotations along with Cu_2O high temperature creep had not been observed directly up to the present. Now, it is important to verify if the change from transient to steady state creep is associated with the formation of a stable microstructure.

2. **Experimental procedure.** — 2.1 SPECIMEN PREPARATION. — Cu_2O rods were prepared by complete oxidation of 99.999 % copper in air at about 1 045 °C. The Cu_2O single crystals were then grown by the zone melted technique in an arc image furnace [5] from a seed with $< 100 >$ orientation under controlled oxygen partial pressure. A further anneal eliminated the CuO precipitates due to the growing method [6]. After orientation from back reflection Laue method the specimens were cut with an Isomet low speed diamond saw [7] : the samples were $2.5 \times 2.5 \times 6$ (± 0.1) mm^3 parallelepiped with six $\{ 100 \}$ faces.

2.2 CREEP. — Mechanical tests were performed in a creep machine already described by Schmidt-Whitley *et al.* [8]. The samples were deformed in compression at 800 °C along the $< 100 >$ axis under controlled flowing argon oxygen mixture. The applied stress is 1 kg/mm^2 (10 MPa) and the strains for each observation of the microstructure of the same sample varied from 2 % to 30 %, the difference between two successive strains being above 5 %.

2.3 OBSERVATION METHODS. — 2.3.1 *Berg-Barrett technique.* — We have observed by Berg-Barrett X ray topography [3, 4] the dislocation substructure and the resultant lattice rotations. We used $< 200 >$ reflecting planes to examine two orthogonal $\{ 100 \}$ faces mechanically and chemically polished a few minutes in a strongly stirred 70 % H_3PO_4 + 30 % HNO_3 mixture. The horizontal divergence of the X ray beam is about 24′. We observe an horizontal distorsion of 0.53 on the topographs due to the fact that the photographic plate is parallel to the incident beam and not to the specimen surface.

We shall quickly recall the source of different types of Berg-Barrett contrasts. The crystal is in Bragg reflexion (θ angle) for the wavelength λ ; we mainly distinguish two kinds of contrasts on the topographs :

1) *An extinction contrast* which results from a local disturbance of the lattice periodicity by a defect ; the

primary extinction is reduced thus giving rise to an enhanced reflectivity power.

2) *An orientation contrast* which results from a local lattice rotation due to the existence of a more or less coarse subboundary. We consider the decomposition of the Ω lattice rotation along three axis (Fig. 1).

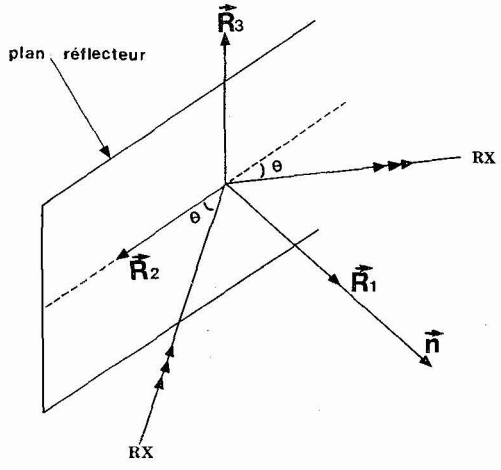

FIG. 1. — Decomposition of any rotation axis along three orthogonal axes R_1, R_2, R_3. These axes give rise to different orientation contrasts.

$\mathbf{R}_1$ normal to the reflecting plane ;

$\mathbf{R}_2$ trace of the reflecting plane with the incidence plane ;

$\mathbf{R}_3$ normal to the incidence plane.

A lattice rotation around the $\mathbf{R}_3$ axis immediately changes the Bragg angle and gives *a rotation contrast* (no reflected ray ; white area on the film). The location of a rotation axis in a sample consists therefore in bringing successively three axis of the crystal in the $\mathbf{R}_3$ position.

An easy measure of the rotation will be made taking advantage of the practically unchanged Bragg angle if the rotation β around the $\mathbf{R}_2$ axis is beyond a critical value ($\lesssim 1°$). In this case the reflected ray is inclined by $2\beta \sin\theta$ in a direction normal to the plane of incidence and gives rise to a *displacement contrast.*

It has to be noticed that a lattice rotation around the $\mathbf{R}_1$ axis is ineffective for contrast formation since it does not change the Bragg angle.

In the present case we used the $\mathbf{R}_3$ axis to exhibit a rotation and the $\mathbf{R}_2$ axis to measure the angle of the rotation ; these two axes are respectively vertical and horizontal in our experiments as well as in our topographs.

2.3.2 *Etch Pits.* — The observation of the dislocation substructure was also studied by optical reflexion microscopy. The etching in a 70 % H_3PO_4 + 30 % HNO_3 is made in a few seconds on a chemically polished sample.

3. **Results.** — 3.1 MICROSTRUCTURE PRIOR DEFORMATION. — The samples exhibit a microstructure with cells elongated along the [001] growth axis. The size of these cells is irregular, the average being about 300 μm. The etching is rather easy and we have verified the coincidence of the revealed substructure with that of the Berg-Barrett topographs (Fig. 2).

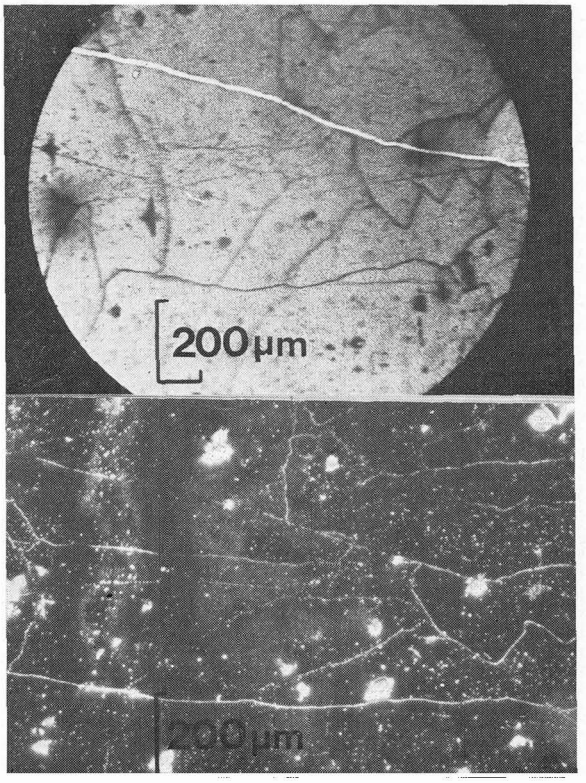

FIG. 2. — Sample prior deformation : comparison of the etch pit substructure and Berg-Barrett topography. An 0.53 horizontal distortion has to be accounted for in the last case.

If we observe the rotations around the [100], [010] and [001] axis, there is no rotation (within the accuracy of the divergence beam : 24′) around the first two axes, but a strong rotation around the [001] axis : figures 3*a* and 4*a* show that the sample is made of three or four subgrains ; 25′, 50′ and 1° 15′ rotations around the [001] displacement axis have been observed between the subgrains, but they can reach 3° for other samples.

The initial substructure is therefore made of big subgrains of about 1 mm which have rotated approximately 1° around the [001] axis. Inside them, we observe cells of about 300 μm which have not rotated (< 24′). At the beginning of the creep we are only interested by misorientation within these subgrains ; after a 10 % strain, we shall not be able to identify the initial subboundaries.

3.2 MICROSTRUCTURE AFTER DEFORMATION. — Whatever may be the strain, we observe a macroscopic deformation of the specimen having two plane sides and two barrel shaped sides (Fig. 5). An observation of the starting sample and of its bent face after a 5 % strain (Fig. 3*a* and *b*) shows a rotation around the [100]

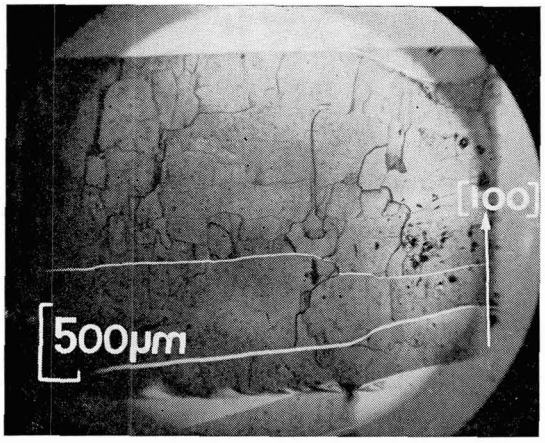

a)

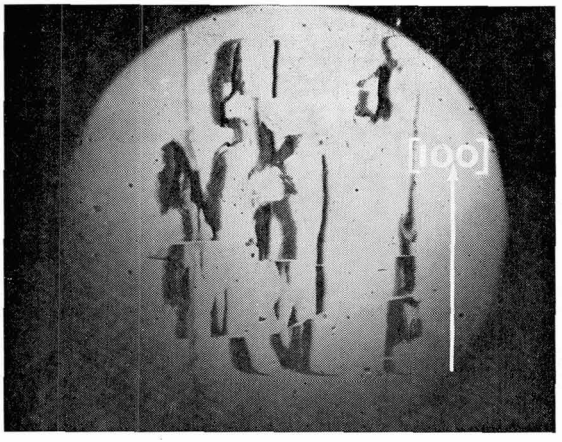

b)

FIG. 3. — Berg-Barrett topographs : (010) bent face, (020) **g**, [100] vertical rotation axis, *a*) starting sample, *b*) after a $\varepsilon \simeq 5\%$ strain we observe a rotation around the [100] axis.

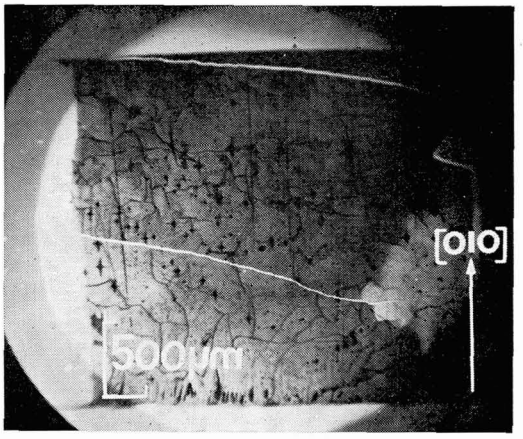

a)

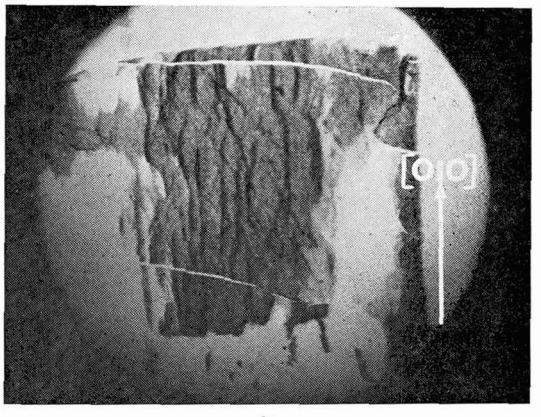

b)

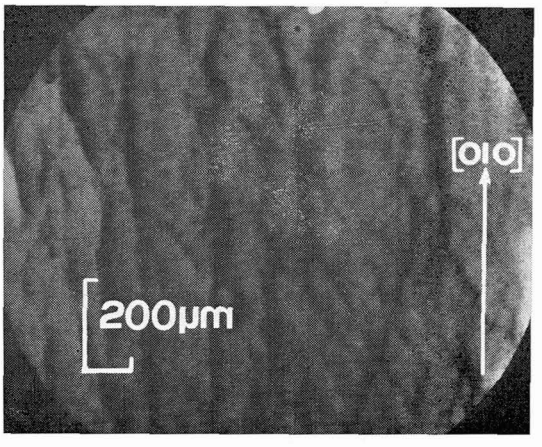

c)

FIG. 4. — Berg-Barrett topographs : (100) plane face, (200) **g**, [010] vertical rotation axis, *a*) starting sample, *b*) after a $\varepsilon \simeq 5$ % strain, *c*) magnification of, *b*) topograph.

axis. An observation of the plane face (Fig. 4*a* and *b*) shows no rotation around the [010] axis ; we can distinguish on figure 4*c* the trace of two glide bands { 011 }, whilst vertical walls parallel to [010] seem to be the traces of the other two glide planes and leave us in expectation of a rotation around this axis. These very constant results are observed from the beginning of the deformation. Going on with creep, we then see a rotation around the [010] axis : it is always smaller than the rotation around the [100] axis, but seems to be the quicker ($\varepsilon \simeq 5$ %) the lower the cristalline perfection is. It begins at a 20 % strain for the sample cristalline perfection of figures 3 and 4.

These qualitative results have been completed by analysis of the displacement contrast : axis [100] and [010] are then horizontal ; it is to be noticed that the distinctness of figure 6 and figure 7 topographs is due to no rotation around the [001] axis which is the direction of the applied stress. Figure 6 clearly shows the increase of the rotations around the [100] axis along with creep : we observe an enhancement of the vertical deviation of the reflected beams and the vanishing of some reflected beams for a 24 % strain. We can estimate the average cell size to be 130 μm for a 15 % strain.

Table I showing the rotations around the [100] axis was made from these topographs ; the results have been checked for other samples. It is to be noticed that these

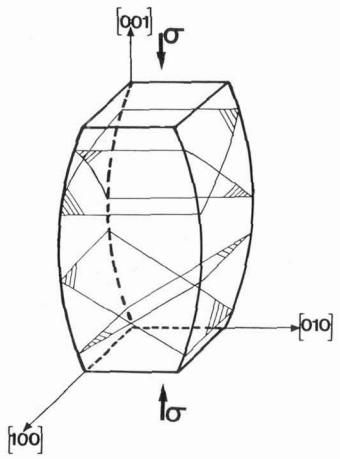

FIG. 5. — Deformed sample : reference axes.

$\delta\theta$ values indicate only local rotations between two adjacent cells ; the rotation $\Delta\theta$ all over the sample, determined from back reflexion Laue pattern, is more important : 5° for a 8 % strain and 12° for a 34 % strain.

TABLE I

Lattice rotations $\delta\theta$ around the [100] axis for various strains ε

ε	5 %	15 %	24 %
$\delta\theta$	15′ to 25′	49′ to 1°15′	> 2°

Figure 7 clearly shows, first the formation of glide planes, then the establishment of a creep substructure. We shall remark that the slight rotation around the [010] displacement axis does not lead to the vanishing of the reflected beam before $\varepsilon \simeq 33$ % (Fig. 7*d*). For this strain the observation of the etch pits (Fig. 8) shows a homogeneous substructure, the average cell size being about 50 μm ; here it concerned a plane face, but the micrograph of a bent face is quite identical. Table II showing rotations around the [010] axis was established from a sample of lower cristalline perfection giving rise to an earlier rotation around the [010] axis than the previous sample.

The whole rotation determined from back reflexion Laue pattern varies from 2° to about 4° for a 27 % strain.

Tables I and II show the importance of the rotation around the [100] axis as compared to the rotation around the [010] axis. This result is likely to be correlated with the macroscopic deformation of the specimen happening along two glide planes in spite of having four possible glide planes [2].

TABLE II

Lattice rotations $\delta\theta$ around the [010] axis for various strains ε

ε	3 %	10 %	27 %
$\delta\theta$	10′	15′	1° to 2°

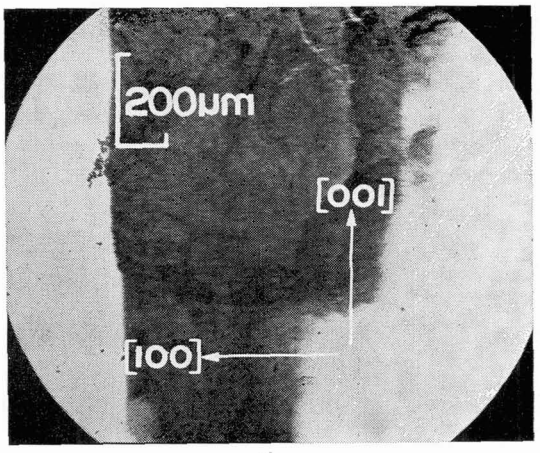

a)

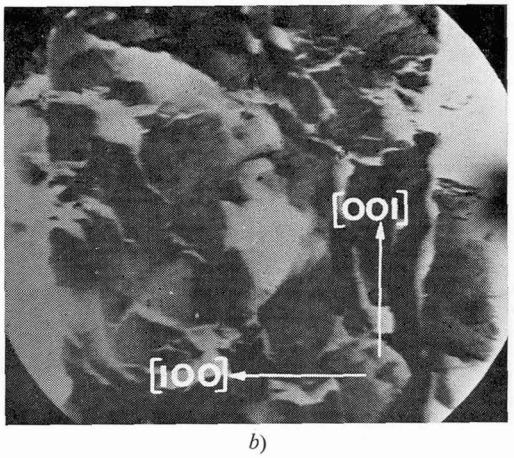

b)

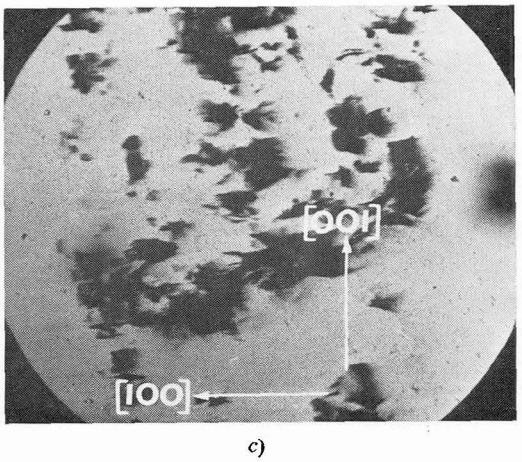

c)

FIG. 6. — Berg-Barrett topographs : increase of the rotations around the [100] axis along with creep, *a)* $\varepsilon \simeq 5$ %, *b)* $\varepsilon \simeq 15$ %, *c)* $\varepsilon \simeq 24$ %, (010) bent face, (020) **g**, horizontal displacement [100] axis.

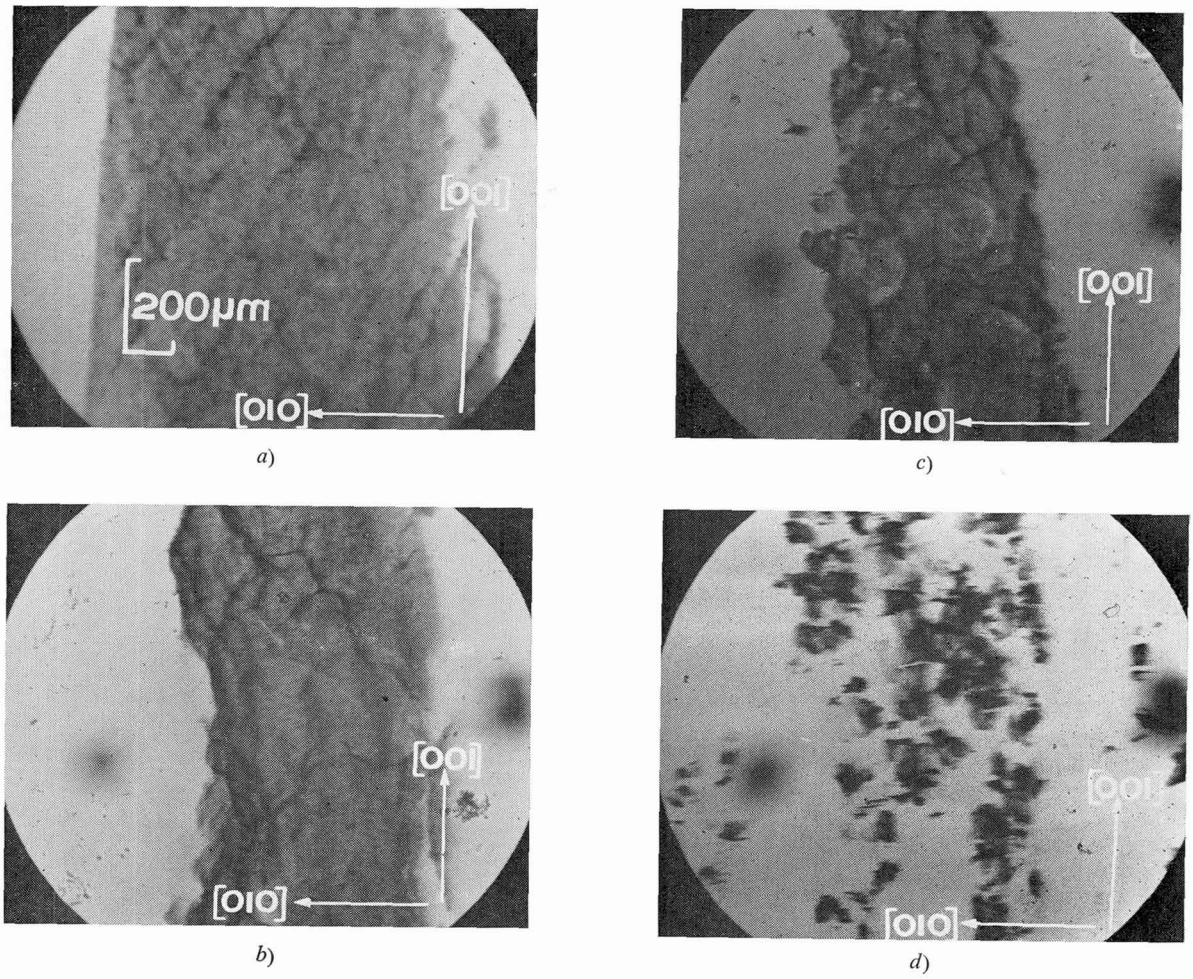

FIG. 7. — Berg-Barrett topographs : observation of the glide planes for, *a*) $\varepsilon \simeq 5$ % and of the establishment of the creep substructure for, *b*) $\varepsilon \simeq 15$ %, *c*) $\varepsilon \simeq 24$ %, *d*) $\varepsilon \simeq 33$ %, horizontal displacement axis [010], (100) plane face.

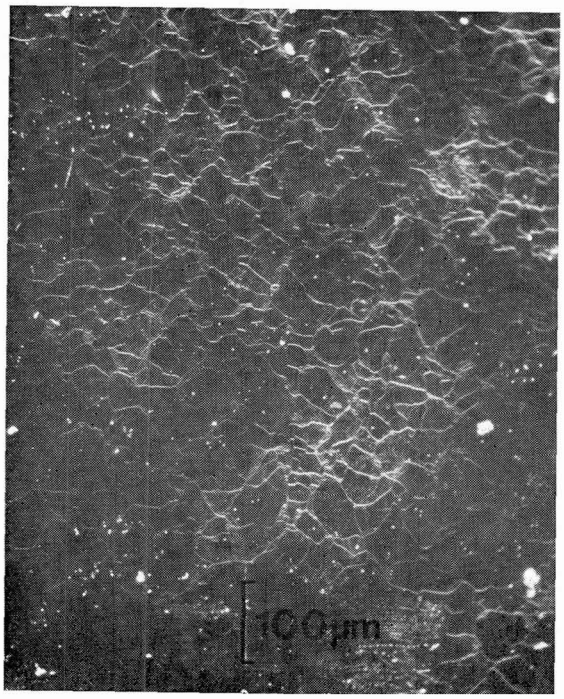

FIG. 8. — Optical reflexion microscopy observation of etch pits after a $\varepsilon \simeq 33$ % strain, (100) plane face.

4. **Conclusion.** — This deformation geometry with four glide planes is very much similar to that of other ionic or ionocovalent crystals of NaCl structure [9], [10]. Along the transient creep ($\varepsilon < 20$ %) we have observed by Berg-Barrett topography the growth of four { 011 } glide planes leading to the formation of a microstructure associated with steady state creep. Nevertheless only two orthogonal planes seem to account for the main part of plastic deformation ; their intersection [100] is the main rotation axis. The two other glide planes intersect along the [010] axis which is the axis of the minor rotation.

We intend to further investigate these studies of microstructure of Cu_2O single crystals after high temperature creep in particular the influence of the direction of the applied stress on glide systems and creep substructure.

Acknowledgments. — The authors wish to acknowledge J. Castaing and Professor J. Philibert for useful comments on this work.

References

[1] MARTINEZ-CLEMENTE, M., BRETHEAU, T., CASTAING, J., *J. Physique* **37** (1976) 895.

[2] BRETHEAU, T., MARHIC, C., SPENDEL, M. et CASTAING, J., to be published in *Phil. Mag.*

[3] NEWKIRK, J. B., *Trans. Metal. Soc. A. I. M. E.*, U. S. A. **215** (1959) 482.

[4] WILKENS, M., *Can. J. Phys.* **45** (1967) 567.

[5] SAURAT, M. et REVCOLEVSCHI, A., *Rev. Int. Hautes Temp. Réfract.* **8** (1971) 291.

[6] SCHMIDT-WHITLEY, R. D., MARTINEZ-CLEMENTE, M. et REVCOLEVSCHI, A., *J. Cryst. Growth* **23** (1974) 113.

[7] BRETHEAU, T., CADOZ, J., DOLIN, C., PELLISSIER, B. et SPENDEL, M., *Ind. Ceram.* **694** (1976) 293.

[8] SCHMIDT-WHITLEY, R. D., MARTINEZ-CLEMENTE, M., CASTAING, J., *Phys. Status Solidi* (a) **27** (1975) 107.

[9] HUTHER, W., REPPICH, B., *Phil. Mag.* **28** (1973) 363.

[10] POIRIER, J. P., *Phil. Mag.* **26** (1972) 713.